Experimentally Validated Reversible Single-Phase Multiwinding Transformer Model for the Accurate Calculation of Low-Frequency Transients

Saeed Jazebi, *Member, IEEE*, and Francisco de León, *Senior Member, IEEE*

***Abstract*—In this paper, a previously published model for the representation of the leakage inductance of multiwinding transformers is enhanced to support accurate calculations of low-frequency transients, including inrush currents, series ferroresonance, and geomagnetic-induced currents. The new circuit is obtained from the principle of duality and, therefore, is physically consistent. The unique characteristic of the improved model is that the very deep saturation behavior of the iron core is properly represented for each winding simultaneously (reversible model) without changing parameters. The hysteresis cycle and iron-core losses are also included. In addition to its reversible terminal behavior coupled with physical consistency, the proposed model can be built with circuit elements available in Electromagnetic Transients Program-type programs, and all of the parameters can be computed from terminal tests. The model is validated by comparing computer simulations versus laboratory measurements for three- and four-winding transformers.**

***Index Terms*—Duality, electromagnetic transients, ferroresonance, geomagnetic-induced current (GIC), inrush currents, multiwinding transformers.**

I. Introduction

MULTIWINDING transformer models have broad applications in the design and development of power systems and power-electronic devices. Several multiwinding transformer models exist in the literature. Among them, the models presented in [1]–[10] need to be acknowledged. The saturation inductance (frequently called "air-core" inductance) and winding resistance, the dominant parameters for transients when the core saturates, are different for each winding since the geometry (at the very least the radius) is different; see [11] and [12]. Therefore, inrush currents, geomagnetic-induced currents (GICs), and ferroresonance occur at different levels of current and voltage for each winding. Laboratory measurements on a four-winding transformer are shown in Fig. 1. This figure demonstrates the significant difference in the transient response of the windings during inrush currents. This attribute is neither reported nor considered in publications dedicated to multiwinding transformer models.

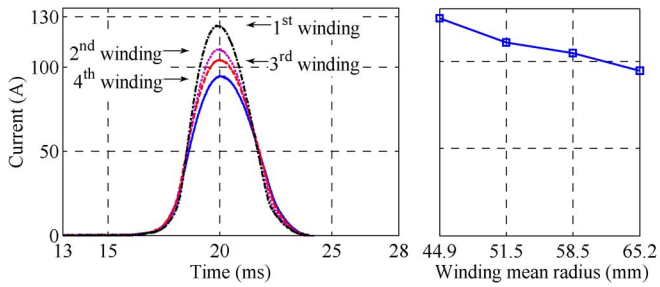

Fig. 1. Inrush current amplitudes for concentric windings with different mean radius. All windings have the same number of turns and conductor cross-sectional area. The saturation inductance and the winding resistance increase for windings with larger radii, which reduce the inrush currents.

Recently, an analytical solution for single-phase two-winding transformers was proposed based on equivalent reluctance circuits [13]. The model accurately considers the deep saturation behavior of the two windings simultaneously and, therefore, the word *reversible* was coined for this model. However, the model of [13] cannot be built with circuit elements available in EMTP-type programs. Thereafter, a dual magnetic-electric model was proposed to overcome this drawback in [14]. The model of [14] is derived from terminal measurements and is easy to implement in any EMTP-type program since it only uses the standard circuit element.

It is known that the terminal behavior of the duality derived transformer models does not always match the terminal measurements performed in the laboratory; see [8] and [14]. The main contribution of this paper is to enhance the terminal behavior of the multiwinding transformer model presented in [8] and [9] to accurately represent the low-frequency behavior of different windings involving very deep saturation.

The equivalent magnetic electrical model of this paper is derived from the principle of duality. Step-by-step guidelines to compute the parameters of the model from measurements are presented. The model includes: leakage inductances, mutual couplings, hysteresis loops, and iron-core losses. The very deep saturation regions of the magnetizing branches are calculated from the solution of the equivalent circuit to match the terminal measurements. The model is compatible with all circuit simulators since only standard circuit elements are needed. The excellent agreement between simulations and laboratory

Manuscript received December 15, 2013; revised March 21, 2014; accepted April 05, 2014. Date of publication May 06, 2014; date of current version January 21, 2015. This work was supported by the U.S. Department of Energy under Grant DEOE 0000072. Paper no. TPWRD-01406-2013.

The authors are with the Department of Electrical and Computer Engineering, NYU Polytechnic School of Engineering, Brooklyn, NY 11201 USA (e-mail: jazebi@ieee.org; fdeleon@nyu.edu).

Color versions of one or more of the figures in this paper are available online at http://ieeexplore.ieee.org.

Digital Object Identifier 10.1109/TPWRD.2014.2319093

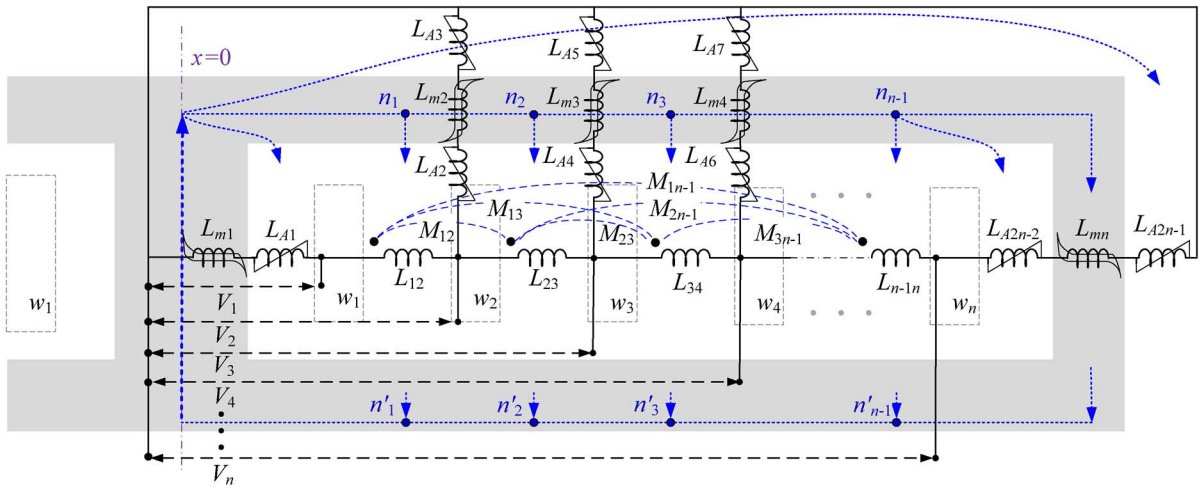

Fig. 2. Direct application of the principle of duality on a multiwinding transformer. Note that due to the symmetry of the equivalent electrical circuit with respect to the $x = 0$ axis, only the right-half side of the transformer window is illustrated.

measurements demonstrates that the model is accurate and perfectly reversible.

This paper deals with single-phase multiwinding transformers. The same methodology will be applied to the multiphase multiwinding model presented in [10] in a forthcoming paper.

II. Modeling Principles

The structure of the model is derived from the direct application of the principle of duality to multiwinding transformers. Fig. 2 illustrates half the window of a shell-type n-winding single-phase transformer. The equivalent electrical circuit is depicted on top of the transformer frame. The leakage inductances are modeled with linear inductors and mutual couplings. The leakage inductances between the windings are represented by L_{ij}. The mutual inductances (M_{ij}) compensate for the missing linking flux between the windings [8], [9]. The iron core is modeled using hysteretic inductors. Also, nonlinear inductors are considered for the contribution of the magnetic energy in the air [14]. The methodology replicates the physical behavior of the magnetic flux for different operating conditions. Therefore, it is in full agreement with the principle of duality and modifies the equivalent circuit for high saturation conditions. This is so because in the operating regions below the knee point (during the short circuit, normal open circuit, and nominally loaded), the value of the air inductances is negligible when compared to the iron-core inductances. However, in deep saturation, the distribution of the magnetic energy completely changes, because a saturated iron core becomes linear with incremental permeability similar to air. Therefore, the magnetic flux is no longer concentrated solely in the iron core, but is distributed in the transformer window and air (see Fig. 3). Under these conditions, the flux between the windings and the core and the flux outside the transformer window become significant since they are comparable to the flux in the core and leakage flux between the windings.

To accurately represent the aforementioned phenomenon, the nonlinear air inductances (inductances L_{A1} to L_{A2n-1} in Fig. 2) are represented with two slopes: zero in normal operating regions and a constant slope in high saturation. Fig. 4 illustrates

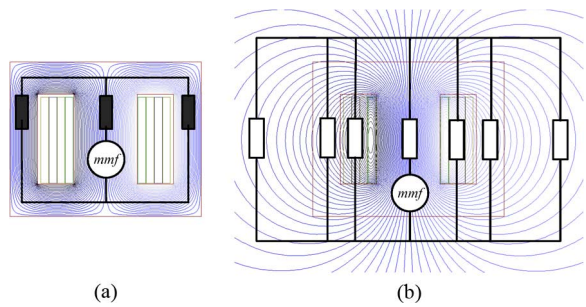

Fig. 3. Magnetic-field strength and the magnetic circuit for an open-circuited transformer: (a) normal operating region and (b) deep saturation region ($\mu_r \rightarrow 1$).

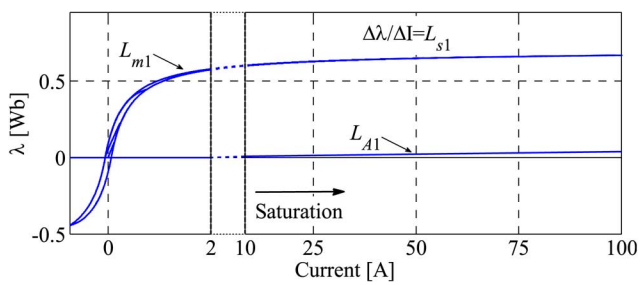

Fig. 4. Magnetizing characteristic of the branch L_{m1} for a 1-kVA 120-V shell-type transformer.

the magnetizing characteristics of the inductor L_{m1} and the air inductance L_{A1}. In this figure, L_{s1} represents the inductance of the linear part (in deep saturation) of the magnetizing curve. The series inductances L_{A1} and L_{m1}; L_{A2}, L_{A3}, and $L_{m2}\ldots$; and L_{A2n-2}, L_{A2n-1}, and L_{mn} could be merged into single inductors. For example, according to the characteristics of L_{A1} shown in Fig. 4, only the high saturation slope of L_{m1} changes to $L_1 = L_{A1}+L_{s1}$, where L_1 is the modified slope of L_{m1} in the high saturation region. Similarly, L_n represents the deep saturation slope of the magnetizing inductor L_{mn} in the model. Then, the winding resistances, core losses, and ideal transformers are added to the circuit of Fig. 2; see Fig. 5 for the final model.

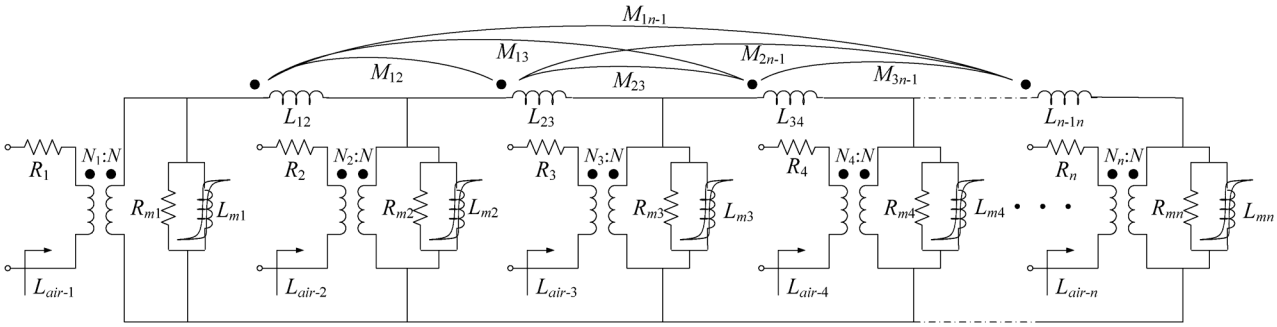

Fig. 5. Reversible multiwinding transformer model including resistances and ideal transformers; $L_{\mathrm{air}-1}, L_{\mathrm{air}-2}, \ldots L_{\mathrm{air}-\mathrm{n}}$ are the saturation inductances of the windings for the modification of the terminal response of the model for the high saturation region.

The principal advantage of this model, which differentiates it from the model of [8], is the computation of the deep saturation inductances of the magnetizing inductors (L_{mn}). Note that according to the equivalent circuits of Figs. 2 and 5, a hysteretic magnetizing inductor is connected in parallel with the terminals of each winding. These n inductors are frequently called magnetizing or nonlinear branches in this paper. The existence of the n branches provides adequate degrees of freedom to correctly characterize the different equivalent inductance values from the terminals in the saturation region.

As noted before, the electromagnetic behavior of the core and air is different under normal operating condition than in deep saturation. Therefore, magnetizing branches are modeled in two steps: First, the nonlinear behavior of the iron core in the nonsaturated region, below the knee point, is considered including hysteresis; second, the linear behavior of the iron core in deep saturation is added. The guidelines for the calculation of the unknown parameters of the model are described in the following subsections.

A. Magnetizing Branches: Hysteresis Curve

In an open-circuited transformer excited with rated voltage, the iron core operates below the knee point, where the value of the magnetizing inductance is substantially larger than the leakage inductances. Hence, the leakage inductances, together with its mutual couplings, are negligible in comparison with the magnetizing inductances. Note that during the standardized open-circuit test with nominal voltage excitation, the magnetic flux is concentrated in the iron core. Therefore, similar hysteresis curve and magnetizing parameters (R_m and L_m) are obtained from measurements on the different windings. This has been demonstrated experimentally by measuring almost the same magnetizing current in all windings when excited with rated voltage, within measuring accuracy.

In the normal operating region, the measured $\lambda_m - i_m$ characteristic could be distributed between the n magnetizing branches considering the leg/yoke geometrical proportions. Since the leakage inductances do not exist, the nonlinear branches of Fig. 2 are effectively in parallel. Note that it is possible to estimate the design details, such as dimensions of the iron core and windings with the method of [15]. Nevertheless, for simplicity, it is assumed that the transformer window is square. Thus, the length of the legs is the same as the length of the yokes. Also, it is assumed that the distances between the neighboring windings are the same. Hence, the leakage fluxes leave the yoke at points located at $1/n, 2/n, \ldots, (n-1)/n$ of the length of the yoke (see nodes $n_1, n_2, \ldots n_{n-1}$ in Fig. 2). Therefore, the limbs are physically divided into $n-2$ regions which result in $L_{m2} = L_{m3} = \ldots = L_{mn-1}$. Besides, $L_{m1} = L_{mn}$, because normally the width of the center leg is twice the width of the side legs and the length of the flux paths are the same (distance between nodes n_1, n_1', and n_{n-1}, n_{n-1}' in Fig. 2). Finally, for the n-winding transformer, the method of [9] is extended as follows:

$$L_{m1} = L_{mn} = \frac{4nL_m}{n+2},\ L_{m2} = L_{m3} = \cdots = L_{mn-1} = 2nL_m \tag{1}$$

where L_m is the magnetizing inductance measured from any winding. Hence, the $\lambda - i$ characteristics of each branch are obtained with the following expressions:

$$\begin{aligned} \lambda_{m1}(k) &= \lambda_{m2}(k) = \cdots = \lambda_{mn}(k) = \lambda_m(k) \\ i_{m1}(k) &= i_{mn}(k) = \frac{(n+2)i_m(k)}{4n} \\ i_{m2}(k) &= i_{m3}(k) = \cdots = i_{mn-1}(k) = \frac{i_m(k)}{2n} \end{aligned} \tag{2}$$

where $\lambda_{mi} - i_{mi}$ is the magnetizing curve of the ith nonlinear branch and k is the kth point of the data. The trapezoidal rule of integration is applied to compute λ_m from the measured terminal voltage obtained from the open-circuit tests. Note that current i_m is measured in the primary (low voltage) winding and the induced voltage is captured at the open-circuited secondary (high voltage) winding.

B. Magnetizing Branches: Deep Saturation Region

The magnetic circuit of an open-circuited transformer consists of several parallel branches connected to a mmf (see Fig. 3). The circuit can be simplified (by series/parallel combinations) resulting in a single nonlinear reluctance with a hysteretic characteristic for normal conditions and linear behavior in deep saturation. The dual electrical representation of this model is a single hysteretic branch. Therefore, the simplest dual representation of a transformer model in the open-circuit condition is a single hysteretic inductor in series with the terminal resistance of the corresponding winding. This could be seen in Fig. 6(a) and (b) for the first and the second windings of a two-winding transformer.

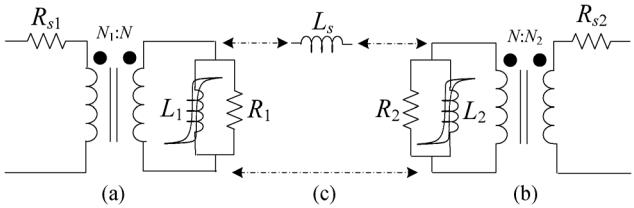

Fig. 6. Infrastructure of a duality-derived π model for a two-winding transformer; (a) the simplest dual representation of the first winding for all open-circuit conditions; (b) the simplest dual representation of the second winding for all open-circuit conditions; (c) addition of the leakage inductance to consider the contribution of the leakage flux during the short-circuit and normal loaded conditions. The joint connection of L_s, L_1, and L_2 affects the open-circuit behavior of the transformer especially in deep saturation.

Note that the leakage inductances do not have a physical existence in open-circuit conditions (because there is no leakage flux when only one winding is energized). However, to simulate the normal operating conditions, a model requires the representation of the leakage flux between the two windings (when at least two windings are energized). To have a unique model in open- and short-circuit conditions, the leakage components need to be added to the circuits according to Fig. 6(c). However, the addition of the leakage inductance affects the behavior of the open-circuit condition of the model of Fig. 6 especially in the deep saturation region.

The leakage inductance is negligible when transformers operate below the knee point in the open-circuit condition. This is so because the magnetizing inductances are much larger than the leakage inductance. For higher excitations, however, the slope of the magnetizing curves decays to the values of the deep saturation inductances $L_1, L_2, \ldots$, and L_n, which are of the same order of magnitude than the leakage inductances. Under these conditions, the effect of the leakage inductance in the equivalent circuit cannot be neglected, considering the fact that leakage inductances are requisites for normal operation and are a part of the model (see Figs. 2 and 5). This causes a mismatch between the terminal measurements and the behavior of the model of [8] in the deep saturation region. To overcome this drawback, general formulas are proposed to precisely calculate $L_1, L_2, \ldots$ and L_n.

1) Derivation of the System Equations: To retrofit the terminal behavior of the model in deep saturation, $L_1, L_2, \ldots, L_n$ needs to be calculated correctly. Fig. 7 illustrates the equivalent circuits seen from different terminals of a three-winding transformer. Note that in each case, the secondary and tertiary windings are open circuited and the damping components are removed for the analysis since only saturation inductances are measured. The primary winding is excited with a hybrid ac/dc voltage source to drive the transformer into deep saturation as recommended in [12]. The modeling technique is based on terminal measurements; therefore, the topology of the model is consistent for transformers with or without tank, magnetic tank shunts, belts, etc. However, the deep saturation inductance measurements are affected in the presence of these transformer parts, which change the values of $L_1, L_2, \ldots, L_n$. The term "air-core inductance" [12] can only be used for an air coil or a transformer without core and tank. Therefore, in this paper, it is

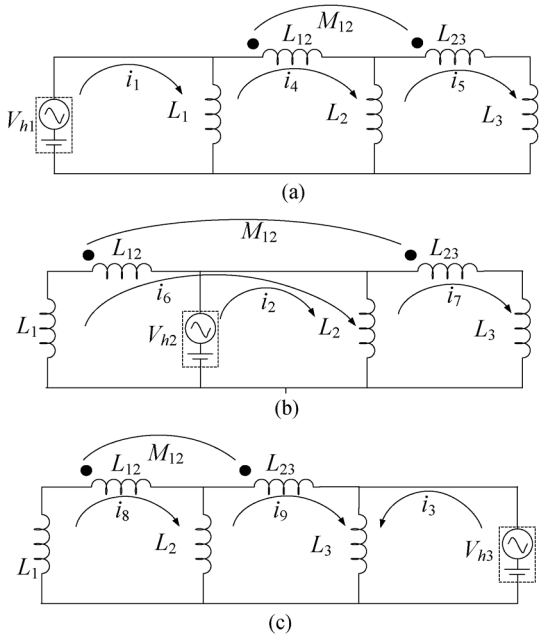

Fig. 7. Equivalent circuits for the calculation of the saturation inductances for a three-winding transformer; simplified circuit seen from (a) the first winding, (b) the second winding, and (c) the third winding.

substituted with "saturation inductance" as in [16]. As the result of the ac/dc excitation, all three magnetizing branches operate in the linear saturated region. Therefore, these branches are represented with the corresponding constant slope part of the deep saturation region (L_1, L_2, and L_3). Fig. 8 illustrates the equivalent circuits seen from the terminals of a four-winding transformer in deep saturation. Similar circuits are derived for the n-winding transformer as shown in Fig. 9.

The first step is to obtain the equivalent inductances seen from the terminals of the model $(L_{\mathrm{air}-1}, L_{\mathrm{air}-2}, \ldots, L_{\mathrm{air}-\mathrm{n}})$ with respect to the variables $L_1, L_2, \ldots, L_n$. The judicious selection of the meshes, including direction and numbering, as illustrated in Figs. 7–9, is essential to obtain simplified equations suitable for generalization. These mesh equations are written for the fundamental components of the voltage and current, where V_i is the fundamental component of the hybrid voltage source V_{hi}, as follows:

$$j\omega[K]_{n^2\times n^2}[I]_{n^2\times 1} = [V]_{n^2\times 1} \quad ,[K] = \begin{bmatrix} A & B \\ B^T & D \end{bmatrix}. \quad (3)$$

The current and voltage vectors are as follows:

$$[I] = [i_1, i_2, i_3, \ldots i_{n^2}]^T \quad ,[V] = [v_1, v_2, \ldots v_n, 0, 0, \ldots 0]^T. \quad (4)$$

The $A_{n\times n}$ matrix for the three-, four-, and n-winding transformers is written as follows:

$$\begin{aligned} [A]_{3\times 3} &= diag[L_1\ L_2\ L_3] \\ [A]_{4\times 4} &= diag[L_1\ L_2\ L_3\ L_4] \\ [A]_{n\times n} &= diag[L_1\ L_2 \cdots\ L_{n-1}\ L_n]. \end{aligned} \quad (5)$$

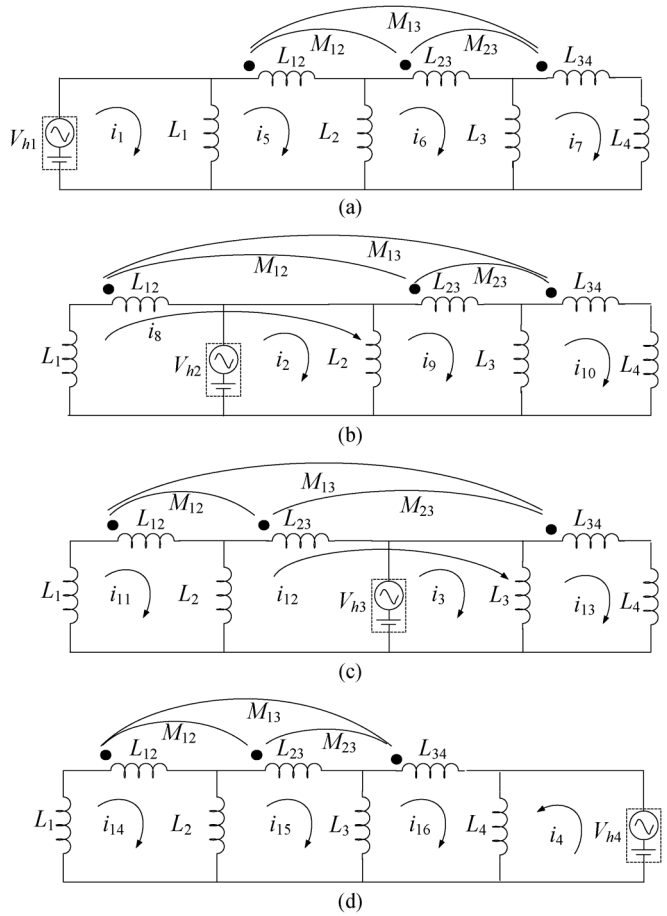

Fig. 8. Equivalent circuits for the calculation of the saturation inductances seen from the four terminals of the four-winding transformer; simplified circuit seen from (a) the first winding, (b) the second winding, (c) the third winding, and (d) the fourth winding.

The elements of $B_{n\times n(n-1)}$ for the three-winding transformer are zeros except for the following components:

$$B_{11}=-L_1,\quad B_{36}=L_3,\quad B_{23}=L_2,\quad B_{24}=-L_2. \tag{6}$$

For the four-winding transformer, the following elements of B are nonzero:

$$\begin{aligned} &B_{11}=-L_1,\quad B_{4,12}=L_4,\quad B_{24}=L_2,\quad B_{25}=-L_2\\ &B_{38}=L_3,\quad B_{39}=-L_3. \end{aligned} \tag{7}$$

The nonzero elements of the B matrix for the n-winding transformer are as follows:

$$\begin{aligned} &B_{11}=-L_1, B_{n,(n-1)n}=L_n\\ &B_{i,(i-1)n}=L_i,\quad B_{i(i-1)n+1}=-L_i,\quad i=2,3,\cdots n-1. \end{aligned} \tag{8}$$

The D matrix is written as follows:

$$[D]_{(n-1)^2\times(n-1)^2}=\begin{bmatrix}[D_a] & & & \\ & [D_a] & & \\ & & \ddots & \\ & & & [D_a]\end{bmatrix} \tag{9}$$

where D_a for the three-winding transformer is

$$[D_a]_{2\times 2}=\begin{bmatrix}L_1+L_2+L_{12} & M_{12}-L_2\\ M_{12}-L_2 & L_2+L_3+L_{23}\end{bmatrix}. \tag{10}$$

For the four-winding transformer, D_a is

$$[D_a]_{3\times 3}=\begin{bmatrix}L_1+L_2+L_{12} & M_{12}-L_2 & M_{13}\\ M_{12}-L_2 & L_2+L_3+L_{23} & M_{23}-L_3\\ M_{13} & M_{23}-L_3 & L_3+L_4+L_{34}\end{bmatrix} \tag{11}$$

and for the n-winding transformer, the D_a matrix is given in (12), as shown at the bottom of the page.

2) Solution of the System Equations: The air-core inductances $(L_{\mathrm{air}-1}, L_{\mathrm{air}-2}, \ldots L_{\mathrm{air-n}})$ seen from each winding are calculated from the following expressions (see Figs. 7–9):

$$L_{\mathrm{air}-1}=\frac{v_1}{j\omega i_1},\quad L_{\mathrm{air}-2}=\frac{v_2}{j\omega i_2},\quad \cdots L_{\mathrm{air-n}}=\frac{v_n}{j\omega i_n}. \tag{13}$$

Equation (13) can be substituted into (3). Note that unknowns $i_{n+1}, i_{n+2}, \ldots, i_n^2$ in (3) do not need to be computed. Therefore, Kron reduction [17] is used to eliminate those variables, and the system order decreases from n^2 to n

$$\begin{aligned} K_{\mathrm{new}}&=A-B\times D^{-1}\times B^T\\ I_{\mathrm{new}}&=[i_1,i_2,\ldots i_n]^T\quad, V_{\mathrm{new}}=[v_1,v_2,\ldots v_n]^T. \end{aligned} \tag{14}$$

$$[D_a]_{(n-1)\times(n-1)}=\begin{bmatrix} L_1+L_2+L_{12} & M_{12}-L_2 & M_{13} & \cdots & M_{1n-2} & M_{1n-1}\\ M_{12}-L_2 & L_2+L_3+L_{23} & M_{23}-L_3 & M_{24} & M_{2n-2} & M_{2n-1}\\ M_{13} & M_{23}-L_3 & L_3+L_4+L_{34} & M_{34}-L_4 & M_{3n-2} & M_{3n-1}\\ \vdots & M_{24} & M_{34}-L_4 & \ddots & & \vdots\\ M_{1n-2} & & & & L_{n-2}+L_{n-1}+L_{n-2,n-1} & M_{n-2,n-1}-L_{n-1}\\ M_{1n-1} & M_{2n-1} & M_{3n-1} & \cdots & M_{n-2,n-1}-L_{n-1} & L_{n-1}+L_n+L_{n-1,n}\end{bmatrix}. \tag{12}$$

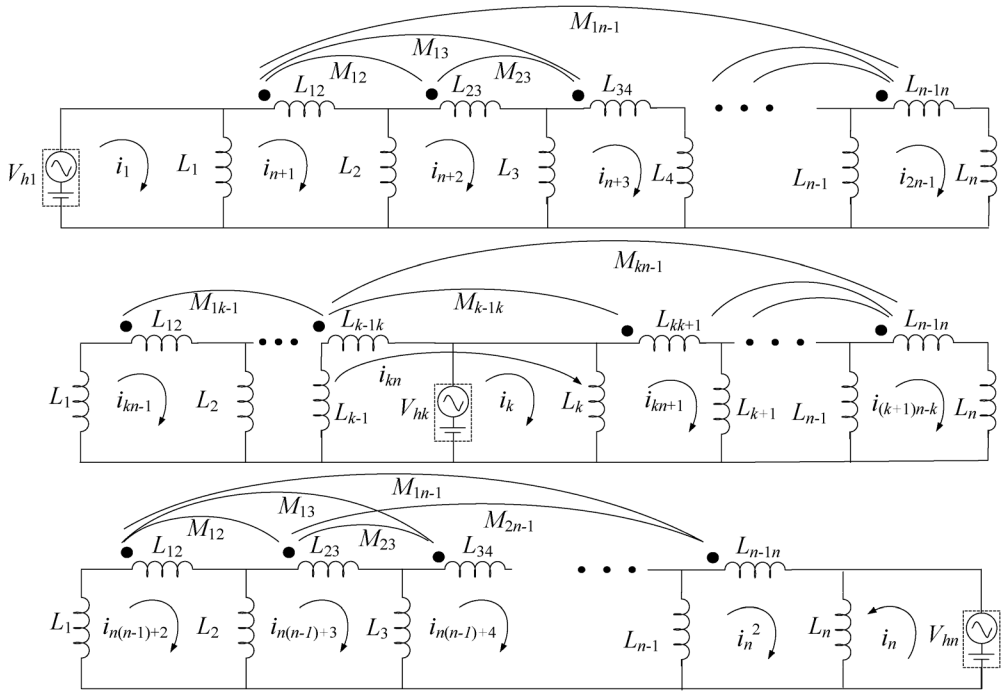

Fig. 9. Simplified equivalent circuits seen from the n terminals of the n-winding transformer for the calculation of the saturation inductances.

The result of this step is a system of n nonlinear equations with n unknowns $L_1, L_2, \ldots, L_n$. Equations (15)–(17), shown at the bottom of the page, are the resulting equations for a three-winding transformer. Note that $L_{\mathrm{air}-1}, L_{\mathrm{air}-2}, \ldots, L_{\mathrm{air}-\mathrm{n}}$ are known parameters which are experimentally measured with a hybrid ac/dc source method as proposed in [12]. Some alternative methods to measure high saturation behavior of transformers could be found in [18]–[21].

To solve the system of nonlinear algebraic equations, the trust-region-reflective algorithm is applied using the embedded Matlab function "lsqnonlin." This function minimizes the set of nonlinear equations with least-square data fitting as follows:

$$\min \|f(L_1, L_2, L_3 \ldots L_n)\|_2^2 = \min \begin{pmatrix} f_1(L_1, L_2, L_3 \ldots L_n)^2 \\ +f_2(L_1, L_2, L_3 \ldots L_n)^2 \\ \vdots \\ +f_n(L_1, L_2, L_3 \ldots L_n)^2 \end{pmatrix}. \quad (18)$$

The parameters are initialized with the saturation inductance values $L_1(0) = L_{\mathrm{air}-1}$, $L_2(0) = L_{\mathrm{air}-2}$, $L_3(0) = L_{\mathrm{air}-3}, \ldots, L_n(0) = L_{\mathrm{air}-\mathrm{n}}$. Finally, the characteristics of the n magnetizing branches computed by (2) are extended from the last point to infinity using $L_1, L_2, \ldots, L_n$ as constant slopes.

C. Leakage Inductances

The leakage inductances are calculated as in [8] by using the standard short-circuit tests performed on each pair of windings independently [22]. The self inductances are

$$L_{i,i+1} = Ls_{i,i+1}, \quad i = 1, 2, \ldots n-1 \quad (19)$$

where $Ls_{i,i+1}$ is the measured leakage inductance between windings i, and $i+1$ and $L_{si,i} = 0$ [8]. Consequently, the mutual inductances M_{ij} are calculated with the following expression:

$$M_{ij} = \frac{Ls_{i,j+1} + Ls_{i+1,j} - Ls_{i,j} - Ls_{i+1,j+1}}{2}. \quad (20)$$

Expressions (19) and (20) have been validated experimentally in [10] for transformers of 96 and 360 MVA. The results are identical to the BCTRAN model proposed in [1].

D. Core Losses

Constant resistors $R_{m1}, R_{m2}, \ldots, R_{mn}$ are added to consider the iron-core losses [23]. The method applied in [9] is extended

$$f_1(L_1, L_2, L_3) = L_1 - \left[L_1^2(L_2 + L_3 + L_{23})\right] / \left[(L_1 + L_2 + L_{12})(L_2 + L_3 + L_{23}) - (M_{12} - L_2)^2\right] - L_{air-1} = 0 \quad (15)$$

$$f_2(L_1, L_2, L_3) = \left[L_2(L_1 + L_{12})(L_3 + L_{23}) - L_2 M_{12}^2\right] / \left[(L_1 + L_2 + L_{12})(L_2 + L_3 + L_{23}) - (M_{12} - L_2)^2\right] - L_{air-2} = 0 \quad (16)$$

$$f_3(L_1, L_2, L_3) = L_3 - \left[L_3^2(L_1 + L_2 + L_{12})\right] / \left[(L_1 + L_2 + L_{12})(L_2 + L_3 + L_{23}) - (M_{12} - L_2)^2\right] - L_{air-3} = 0 \quad (17)$$

for the n-winding transformers. The following equations are obtained with the same assumptions presented in Section II-A:

$$R_{m1}=R_{mn}=\frac{n^2R_m}{2}\quad R_{m2}=R_{m3}=\cdots=R_{mn-1}=\frac{n^2R_m}{n+2} \tag{21}$$

where R_m is the equivalent resistance computed from the standard open-circuit measurements to represent the iron-core losses.

III. Model Validation

Reversible models for three- and four-winding transformers are developed and validated in this section. The models are implemented for a 1-kVA, 120 V, 4-winding isolation transformer. The complete data, such as iron-core dimensions, leakage inductances between different windings, saturation inductances and resistances of different windings, etc. are available in [14]. The reversible model is compared with the conventional model (called nonreversible model) and measurements for validations in different transient conditions.

In the nonreversible model, all parameters are derived according to the guidelines presented in previous sections except the nonlinear branches. In this model, the magnetizing characteristics are extended without the corrections provided in Section II-B. The saturation inductance of the innermost winding is used to adjust the model parameters which give the correct transient behavior of the innermost winding. Note that the same winding resistances are used in both models. Therefore, the performance differences are only due to the use of the wrong saturation inductances in the traditional model.

A. Three-Winding Model

The model for the three-winding transformer is obtained from the first three windings of the four-winding transformer under study. The fourth winding is left disconnected.

1) Inrush Currents: The transformer is energized through a switch that closes when the voltage of the sinusoidal source is crossing zero. The transformer is demagnetized before each experiment. Fig. 10 illustrates the accuracy of the reversible model in comparison to the nonreversible model. In this case, the nonreversible model overestimates the inrush currents by 21.5%, and 22.9%, for the second and the third windings, respectively. The comparison of the results for inrush currents is presented in Table I. The differences between the reversible model results and measurements are about 5%.

2) Ferroresonance: For ferroresonance experiments, a 44-μF series capacitance is connected between the source and the transformer terminal. The transformer is completely demagnetized, and the capacitor is discharged before each measurement. The simulation results are compared to measurements in Table II. One can observe that the simulation results are in good agreement with the laboratory measurements. The same tests are performed for the 22-μF and 66-μF capacitors, and satisfactory results with errors less than 5% are achieved. EMTP simulations show that the nonreversible model is also correct for the calculation of ferroresonance. The overall differences between the reversible and nonreversible models are less than 2%.

3) Geomagnetic Induced Currents: Geomagnetic-induced currents (GICs) cause a *dc* potential on the surface of the earth.

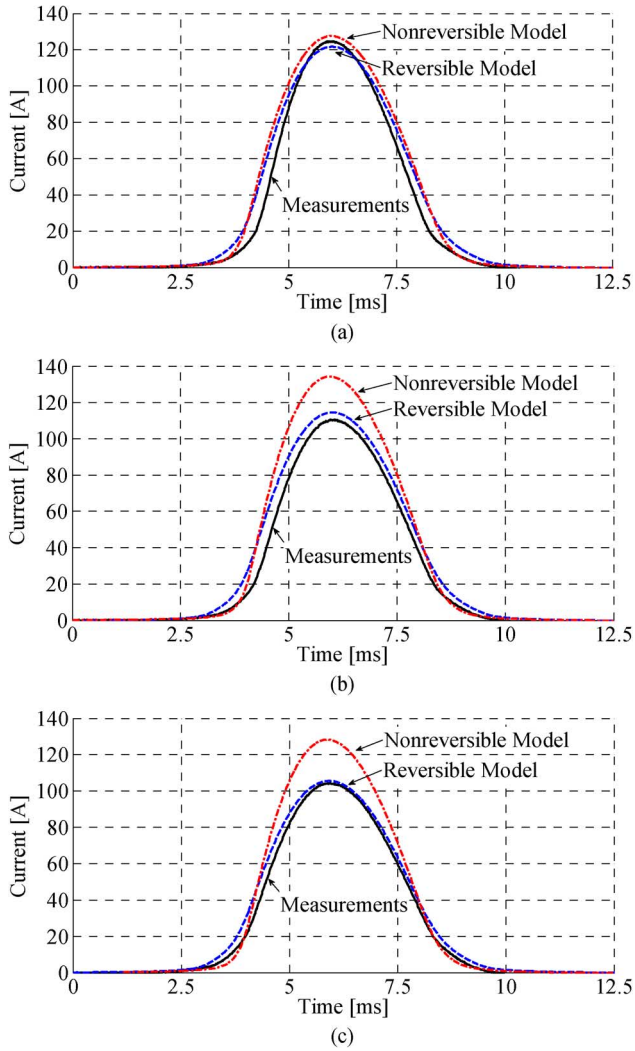

Fig. 10. First peak of inrush currents to validate the three-winding model: (a) innermost winding, (b) inner winding, and (c) outer winding.

TABLE I
Comparison of Inrush Current Peak Values for the Three-Winding Transformer

Winding	Meas. [A]	Nonrev. [A]	Diff. (%)	Rev. [A]	Diff. (%)
1st	124.4	127.6	2.6	121.7	2.1
2nd	110.6	134.4	21.5	114.5	3.5
3rd	104.5	128.4	22.9	105.6	1.0

TABLE II
Maximum Temporary Overvoltage Measured and Simulated for the Three-Windings Transformer and a 44-μF Capacitor (in volts)

Winding	Meas. [V]	Nonrev. [V]	Diff. (%)	Rev. [V]	Diff. (%)
1st	226.5	213.9	5.6	216.1	4.6
2nd	226.4	212.2	6.3	216.4	4.4
3rd	223.5	214.7	3.9	216.5	3.1

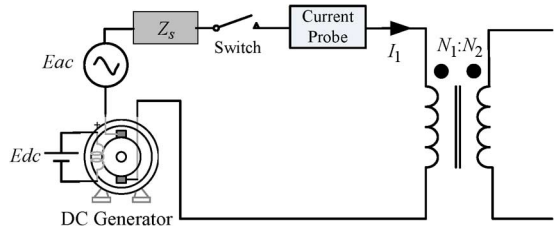

Fig. 11. Laboratory test setup for the GICs.

TABLE III
COMPARISON OF GICS' PEAK VALUES FOR THE THREE-WINDINGS TRANSFORMER

Winding	V_{dc} [V]	Meas. [A]	Nonrev. [A]	Diff. (%)	Rev. [A]	Diff. (%)
1st	4.09	46.4	47.4	2.1	44	5.1
2nd	3.59	39.9	43.4	8.0	37.7	5.5
3rd	4.74	44.8	51.3	18.7	44.5	0.7

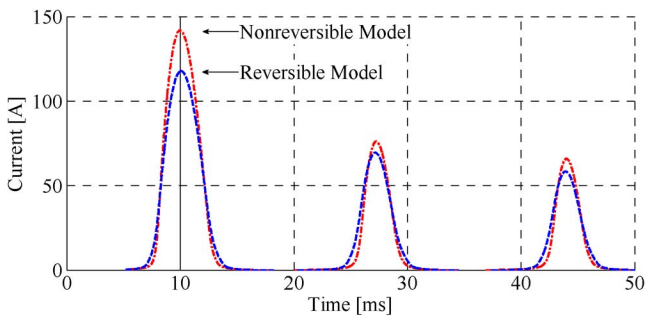

Fig. 12. Inrush current when transformer coils are drawing GICs. Note that due to the lack of space, only the behavior of the outer winding is depicted.

Therefore, during GIC, the transformer neutral is biased with a dc voltage [24]. This condition is simulated in the laboratory and EMTP with a hybrid dc/ac excitation. The hybrid voltage source includes a dc generator in series with an ac source. The dc voltage could be controlled with the field excitation of the generator. The hybrid source is connected to the primary terminal of the transformer while the secondary terminal is open circuit. The schematic diagram of the laboratory setup is presented in Fig. 11. The switch is always closed in this experiment.

Simulations results for the nonreversible and the reversible models are compared versus measurements in Table III. One can see a good agreement between the reversible model and measurements. The nonreversible model shows relative errors of 8%, and 18.8% with respect to the measurements.

4) GIC + Energization: One of the extreme cases of inrush currents could occur when the transformer is energized on the zero crossing of the voltage while the neutral of the transformer is biased by GICs. This phenomenon is simulated with the nonreversible and the reversible models (see Fig. 11 for the simulated circuit). The results are compared for the three-winding transformer model. The nonreversible model predicts the inrush currents with 16.3%, and 20.5% errors for the inner and outer windings, when compared to the reversible model. Fig. 12 shows the simulation results for the outer winding. These results show the significance of the reversible model for extreme cases with higher degrees of saturation.

TABLE IV
COMPARISON OF INRUSH CURRENT PEAK VALUES FOR THE FOUR-WINDING TRANSFORMER

Winding	Meas. [A]	Nonrev. [A]	Diff. (%)	Rev. [A]	Diff. (%)
1st	124.4	123.1	1.0	121.2	2.6
2nd	110.6	131.8	19.2	111.7	1.0
3rd	104.5	127.8	22.3	100.2	4.1
4th	94.6	117.4	24.1	93.8	0.8

TABLE V
MAXIMUM TEMPORARY OVERVOLTAGE MEASURED AND SIMULATED FOR THE FOUR-WINDINGS TRANSFORMER AND A 44-μF CAPACITOR (in volts)

Winding	Meas.	Nonrev.	Diff. (%)	Rev.	Diff. (%)
1st	226.5	214.3	5.4	216.9	4.2
2nd	226.4	214.2	5.4	216.1	4.5
3rd	223.5	214.3	4.1	215.7	3.5
4th	221.9	213.4	3.8	214.4	3.4

TABLE VI
COMPARISON OF GICS' PEAK VALUES FOR THE FOUR-WINDINGS TRANSFORMER

Winding	V_{dc} [V]	Meas. [A]	Nonrev. [A]	Diff. (%)	Rev. [A]	Diff. (%)
1st	4.09	46.4	46.2	0.4	47.3	1.9
2nd	3.59	39.9	42.4	6.3	40.3	1.0
3rd	4.74	44.8	50.2	12.0	46.1	2.9
4th	4.72	42.6	47.3	11.0	43.8	2.8

B. Four-Winding Model

The reversible model is validated for the four-winding transformer under inrush current, ferroresonance, and GIC. The results are compared to the nonreversible model and measurements in Tables IV–VI. The great agreement between the results of simulations for the reversible model and laboratory measurements for all of the windings demonstrates the effectiveness of the reversible model (all differences are less than 5%). On the other hand, the nonreversible model does not properly represent the behavior of all four windings simultaneously. The errors range from a few percent and up to 24%.

IV. CONCLUSION

The model of [8] and [9] has been retrofitted to produce a reversible model for multiwinding transformers. Analytical formulae have been derived to calculate the required parameters from terminal tests. The model can be easily implemented in EMTP-type programs for n-winding transformers since all components are available in their library. The model has been validated by comparing measurements and simulations for three- and four-winding transformers for inrush currents, ferroresonance, and GICs.

The results show the necessity of the proposed improvement to compute transients involving deep saturation. The model is physically sound and very simple to implement without access to the construction geometry and material information of the transformer. All model parameters can be computed from terminal tests.

REFERENCES

[1] V. Brandwajn, H. W. Dommel, and I. I. Dommel, "Matrix representation of three-phase N-winding transformers for steady-state and transient studies," *IEEE Trans Power App. Syst.*, vol. PAS-101, no. 6, pp. 1369–1378, Jun. 1982.

[2] V. A. Niemela, G. R. Skutt, A. M. Urling, Y. Chang, T. G. Wilson, H. A. Owen, and R. C. Wong, "Calculating the short-circuit impedances of a multiwinding transformer from its geometry," in *Proc. IEEE Power Electron. Spec. Conf.*, 1989, pp. 607–617.

[3] H. Mohseni, "Multi-winding multi-phase transformer model with saturable core," *IEEE Trans. Power Del.*, vol. 6, no. 1, pp. 166–173, Jan. 1991.

[4] A. Schellmanns, K. Berrouche, and J. Keradec, "Multiwinding transformers: A successive refinement method to characterize a general equivalent circuit," *IEEE Trans. Instrum. Meas.*, vol. 47, no. 5, pp. 1316–1321, Oct. 1998.

[5] R. W. Erickson and D. Maksimovic, "A multi-winding magnetics model having directly measurable parameters," in *Proc. IEEE Power Electron. Spec. Conf.*, 1998, pp. 1472–1478.

[6] J. Wang, A. F. Witulski, J. L. Vollin, T. K. Phelps, and G. I. Gardwell, "Derivation, calculation and measurement of parameters for a multi-winding transformer electrical model," in *Proc. IEEE Appl. Power Electron. Conf. Expo.*, 1999, pp. 220–226.

[7] J. M. Lopera, M. J. Prieto, A. M. Pernia, and F. Nuno, "A multiwinding modeling method for high frequency transformers and inductors," *IEEE Trans. Power Electron.*, vol. 18, no. 3, pp. 896–906, May 2003.

[8] C. Álvarez-Mariño, F. de León, and X. M. López-Fernández, "Equivalent circuit for the leakage inductance of multi-winding transformers: Unification of terminal and duality models," *IEEE Trans. Power Del.*, vol. 27, no. 1, pp. 353–361, Jan. 2012.

[9] F. de León and J. A. Martinez, "Dual three-winding transformer equivalent circuit matching leakage measurements," *IEEE Trans. Power Del.*, vol. 24, no. 1, pp. 160–168, Jan. 2009.

[10] M. Lambert, M. Martínez-Duró, J. Mahseredjian, F. de León, and F. Sirois, "Transformer leakage flux models for electromagnetic transients: Critical review and validation of a new model," *IEEE Trans. Power Del.*, accepted for publication.

[11] C. M. Arturi, "Transient simulation and analysis of a three-phase five-limb step-up transformer following and out-of-phase synchronization," *IEEE Trans. Power Del.*, vol. 6, no. 1, pp. 196–207, Jan. 1991.

[12] F. de León, S. Jazebi, and A. Farazmand, "Accurate measurement of the air-core inductance of iron-core transformers with a non-ideal low-power rectifier," *IEEE Trans. Power Del.*, vol. 29, no. 1, pp. 294–296, Feb. 2014.

[13] S. E. Zirka, Y. I. Moroz, C. M. Arturi, N. Chiesa, and H. K. Høidalen, "Topology-correct reversible transformer model," *IEEE Trans. Power Del.*, vol. 27, no. 4, pp. 2037–2045, Oct. 2012.

[14] S. Jazebi, F. de León, A. Farazamand, and D. Deswal, "Dual reversible transformer model for the calculation of low-frequency transients," *IEEE Trans. Power Del.*, vol. 28, no. 4, pp. 2509–2517, Oct. 2013.

[15] S. D. Mitchell and J. S. Welsh, "Initial parameter estimates and constraints to support gray box modeling of power transformers," *IEEE Trans. Power Del.*, vol. 28, no. 4, pp. 2411–2418, Oct. 2013.

[16] M. Lambert and J. Mahseredjian, "Electromagnetic transient-type transformer models for geomagnetically-induced current (GIC) studies," Palo Alto, CA, USA, 3002000832, Nov. 2013.

[17] G. Kron, *Tensor Analysis of Networks*. New York: Wiley, 1939.

[18] E. P. Dick and W. Watson, "Transformer models for transient studies based on field measurements," *IEEE Trans Power App. Syst.*, vol. PAS-100, no. 1, pp. 409–418, Jan. 1981.

[19] C. G. A. Koreman, "Determination of the magnetizing characteristic of three-phase transformers in field tests," *IEEE Trans. Power Del.*, vol. 4, no. 3, pp. 1779–1785, Jul. 1989.

[20] S. Abdulsalam, W. Xu, W. L. A. Neves, and X. Liu, "Estimation of transformer saturation characteristics from inrush current waveforms," *IEEE Trans. Power Del.*, vol. 21, no. 1, pp. 170–177, Jan. 2006.

[21] S. Calabro, F. Coppadoro, and S. Crepaz, "The measurement of the magnetizing characteristics of large power transformers and reactors through D.C. excitation," *IEEE Trans. Power Del.*, vol. PWRD-1, no. 4, pp. 224–234, Oct. 1986.

[22] *IEEE Standard Test Code for Dry-Type Distribution and Power Transformers, Recognized as an American National Standard (ANSI)*, IEEE Standard C57.12.91-1995, 1995.

[23] Slow Transients Task Force of the IEEE, Modeling and Analysis of System Transients Using Digital Programs Working Group, "Modeling and analysis guidelines for slow transients–Part III: The study of ferroresonance," *IEEE Trans. Power Del.*, vol. 15, no. 1, pp. 255–265, Jan. 2000.

[24] R. A. Walling and A. H. Khan, "Characteristics of transformer exciting current during geomagnetic disturbances," *IEEE Trans. Power Del.*, vol. 6, no. 4, pp. 1707–1714, Oct. 1991.

Saeed Jazebi (S'10–M'14) was born in 1983 in Kerman, Iran. He received the B.Sc. degree in electrical engineering from Shahid Bahonar University, Kerman, Iran, in 2006, the M.Sc. degree in electrical engineering from Amirkabir University of Technology, Tehran, Iran, in 2008, and the Ph.D. degree in electrical engineering from NYU Polytechnic School of Engineering, Brooklyn, NY, USA, in 2014.

He is continuing his research as a Postdoctoral Fellow at NYU Polytechnic School of Engineering. His fields of interest include electromagnetic design, modeling and simulation of electrical machines and power system components, statistical pattern-recognition applications in power engineering, power system protection, and power quality.

Francisco de León (S'86–M'92–SM'02) received the B.Sc. and the M.Sc. (Hons.) degrees in electrical engineering from the National Polytechnic Institute, Mexico City, Mexico, in 1983 and 1986, respectively, and the Ph.D. degree in electrical engineering from the University of Toronto, Toronto, ON, Canada, in 1992.

He has held several academic positions in Mexico and has worked for the Canadian electric industry. Currently, he is an Associate Professor at the NYU Polytechnic School of Engineering, Brooklyn, NY, USA. His research interests include the analysis of power phenomena under nonsinusoidal conditions, the transient and steady-state analyses of power systems, the thermal rating of cables and transformers, and the calculation of electromagnetic fields applied to machine design and modeling.